



## Enhancement of vacuum birefringence with pump laser of flying focus

Bufan Jin <sup>1,2</sup> and Baifei Shen <sup>2,\*</sup>

<sup>1</sup>*School of Physical Science and Technology, Soochow University, Suzhou 215006, China*

<sup>2</sup>*Department of Physics, Shanghai Normal University, Shanghai 200234, China*



(Received 7 August 2022; revised 4 June 2023; accepted 9 June 2023; published 27 June 2023)

Vacuum birefringence is one of the most fascinating properties of quantum electrodynamics. In laser-induced vacuum polarization signatures, the interaction length is usually limited by the pump laser's Rayleigh length and temporal length. Here, we show that a flying focus pump with focus velocity  $-c$  can overcome the short interaction length of the tightly focused pump laser, providing high intensity and long interaction length at the same time, which may lead to the experimental detection of vacuum birefringence.

DOI: [10.1103/PhysRevA.107.062213](https://doi.org/10.1103/PhysRevA.107.062213)

### I. INTRODUCTION

Quantum electrodynamics (QED) predicts the virtual electron-positron pair creation from the vacuum [1,2]. The polarization of these pairs modifies the propagation of light, and photon-photon scattering can happen even in the vacuum. One of the most famous signatures of QED is vacuum birefringence [3–5]. After a linearly polarized probe laser passes through the strong pump field, perpendicularly polarized scattering photons can be generated, resulting in induced ellipticity for the probe. So far this effect has not been detected in the laboratory because the signal is strongly suppressed by powers of the critical field  $I_{cr} = 2.3 \times 10^{29} \text{ W cm}^{-2}$ . Motivated by the development of ultrastrong electromagnetic fields [6–8], there have been many proposals to detect vacuum birefringence, where the pump field can be a constant magnetic field of a few teslas [9–11], or an ultrastrong laser field to the order of  $10^{23} \text{ W cm}^{-2}$  [12–15]. Though the laser can generate a much stronger background field, the interaction length is much smaller, usually limited by the pump laser's temporal length and Rayleigh length [15].

Flying focus is a newly developed technique for controlling the trajectory of peak laser intensity [16,17]. It was first experimentally demonstrated with a chromatic focusing system combined with chirped laser pulses [16]. Alternate techniques include using a Kerr lens [18] and an axiparabola-echelon pair [19]. Recently, the exact solutions of a flying focus with arbitrary focal velocity were derived [20]. The controlled focal velocity enables a wide range of applications that require velocity matching and a high-intensity interaction over an extended distance [20], including laser wakefield acceleration [19], radiation reaction [21], and nonlinear Thomson scattering [22].

Here, we show that in the laser-induced vacuum polarization effect, a flying focus pump with the focus velocity  $-c$  can overcome the limitation of the tightly focused laser's short Rayleigh length, greatly enhancing the signal when the

pump's temporal length is larger than its Rayleigh length. The physical reason is that the probe laser can always experience the most intense part of the pump laser's spatial profile, thereby allowing for a long pump pulse in the detection of vacuum birefringence, having the advantage of providing both high intensity and long interaction length.

### II. ANALYSIS OF VACUUM BIREFRINGENCE WITH THE FLYING FOCUS PUMP

References [21,23] describe the flying focus beam with the focus moving backwards at the speed of light compared to the laser propagation direction (the exact solutions of a flying focus with arbitrary focal velocity can be seen in [20]). We employ this solution to model the flying focus beam, as it satisfies the free Maxwell's equations exactly, and precisely fits the physical situation we consider. In what follows, we work in Gaussian units  $\epsilon_0 = 1$ ,  $c = 1$ ,  $\hbar = 1$ . From the standpoint of the generation of an arbitrarily structured laser [24], for the vacuum wave equation

$$(\partial_x^2 + \nabla_{\perp}^2 - \partial_t^2)A_{\perp}(x, r, t) = 0, \quad (1)$$

the field can be expressed as the integral over varying property, such as frequency  $k$ . To describe the moving focus, upon performing the Galilean change of variables  $\eta = t - x$  and  $\phi = t + x$ , the transverse components of the four-vector potential at the radial position  $r$  can be expressed as

$$A_{\perp}(\eta, r, \phi) = \int \tilde{A}_{\perp}(\eta, r) e^{-ik\phi} dk, \quad (2)$$

where  $\tilde{A}_{\perp}$  satisfies

$$(\nabla_{\perp}^2 + 2ik\partial_{\eta/2})\tilde{A}_{\perp} = 0. \quad (3)$$

This equation takes the same form of the paraxial wave equation for the Gaussian beams, with the solution

$$\tilde{A}_{\perp} = f(k) \frac{1}{1 + i\eta'/x_0} \exp\left[-\frac{r^2}{w_0^2(1 + i\eta'/x_0)}\right], \quad (4)$$

where  $\eta' = \eta/2$  is the spatiotemporal variable which describes the movement of the focus,  $w_0$  is the beam waist,

\*bfshen@shnu.edu.cn

$x_0 = 0.5kw_0^2$  is the Rayleigh length, and  $f(k)$  is an arbitrary function that describes the spectral profile. As an example, we assume a Gaussian spectral profile  $f(k) = \exp[-(k - k_0)^2\tau^2/4]$ . In general, Eq. (2) contains spatial-temporal coupling terms, and cannot be written analytically. However, for the pulse with many periods, the integration over frequencies can be well estimated as the use of a Gaussian temporal shape. For calculation simplicity, we consider the special case of an isodiffracting pulse [25], where all the frequency components have the same Rayleigh range. Thus Eq. (2) can be easily carried out [26]:

$$A_{\perp}(\eta, r, \phi) = \frac{1}{1 + i\eta'/x_0} \exp\left[-\frac{r^2}{w_0^2(1 + i\eta'/x_0)}\right] \times \exp\left[-\left(\phi - \frac{r^2}{2\eta' - 2ix_0}\right)^2 / \tau^2\right] e^{-ik_0\phi}. \quad (5)$$

This shows that the duration of the pulse is involved in the spatial distribution of the pulsed beam. When  $r^2/(x_0\tau) \ll 1$ , this spatially dependent term can be safely neglected. In our situation, the transverse size of the interaction region is much smaller than the flying focus laser's waist, and the beam has many periods, so that this condition is always satisfied, and we have

$$A_{\perp}(\eta, r, \phi) = \frac{1}{1 + i\eta'/x_0} \exp\left[-\frac{r^2}{w_0^2(1 + i\eta'/x_0)}\right] \times \exp(-\phi^2/\tau^2) e^{-ik_0\phi}. \quad (6)$$

As discussed in [21], this flying focus laser has almost the same energy and intensity as the traditional Gaussian beam of the same  $w_0$  and  $\tau$ .

Now we employ this flying focus beam to enhance the vacuum birefringence signal. We consider the scenario of the head-on collisions between an optical laser pump and a x-ray free-electron laser (XFEL) probe. This prospect was first proposed by [27], and is further analyzed in many papers such as [28,29]. To maximize the vacuum birefringence effect, the polarization angle between the two beams is  $\pi/4$ , and the intersection angle between the propagation directions is  $\pi$  [27]. Let the two initial pulses be

$$\mathbf{E}_X = A_X(r', x')h_X(t - x')e^{-i(\omega_X t - k_X x')} \mathbf{e}_z, \quad (7)$$

$$\mathbf{E}_L = A_L(r', t - x')h_L(t + x')e^{-i(\omega_L t + k_L x')} \sqrt{2}(\mathbf{e}_y + \mathbf{e}_z)/2, \quad (8)$$

where  $h_X(x) = \exp(-x^2/\tau_X^2)$ ,  $h_L(x) = \exp(-x^2/\tau_L^2)$  describe the Gaussian temporal shape with the length  $\tau_X$ ,  $\tau_L$ . The optical pump laser  $A_L(r', t - x')$  takes the flying focus envelope in Eq. (6) with the waist  $w_L$ , and the XFEL probe takes the traditional Gaussian envelope  $A_X(r', x')$  with the waist  $w_X$ . Here we neglect the terms with the same order of those neglected in the paraxial approximation for the Gaussian beams. The two beams move in the opposite direction, while the pump laser's focus moves in the same direction as the XFEL probe.

In classical theory, photons cannot interact with each other, as Maxwell equations are linear. However, QED shows that the vacuum is full of virtual electron-positron

pairs, and is in fact nonlinear. The Euler-Heisenberg Lagrangian [1,2] includes such fermion dynamics to one-loop order. The lowest-order Euler-Heisenberg Lagrangian corresponding to four-photon interaction is

$$L = \frac{1}{8\pi}(E^2 - B^2) + \frac{\xi}{8\pi}[(E^2 - B^2)^2 + 7(\mathbf{E} \cdot \mathbf{B})^2], \quad (9)$$

where  $\xi = e^4/45\pi m^4$ ,  $e$  is the electron charge, and  $m$  is the electron mass. This expression is valid for amplitude much less than the critical field, and frequency much less than the electron mass. A modified wave equation can be derived from the effective Lagrangian density,

$$\left(\nabla^2 - \frac{\partial^2}{\partial t^2}\right)\mathbf{E} = 4\pi\mathbf{J}, \quad (10)$$

where the vacuum current is

$$\mathbf{J} = \frac{\partial}{\partial t}\left(\frac{\partial\mathbf{P}}{\partial t} + \nabla \times \mathbf{M}\right) - \nabla(\nabla \cdot \mathbf{P}), \quad (11)$$

with the polarization  $\mathbf{P} = \xi[2(E^2 - B^2)\mathbf{E} + 7(\mathbf{E} \cdot \mathbf{B})\mathbf{B}]/4\pi$  and magnetization  $\mathbf{M} = \xi[-2(E^2 - B^2)\mathbf{B} + 7(\mathbf{E} \cdot \mathbf{B})\mathbf{E}]/4\pi$ .

Therefore photon-photon scattering is treated in a "quantum-vacuum-modified" classical equation approach [13,30], corresponding to the four-wave coupling process. The total field can be expressed as  $\mathbf{E}_L + \mathbf{E}_X + \mathbf{E}_S$ , where  $\mathbf{E}_X$ ,  $\mathbf{E}_L$  are the initial pulses that satisfy the Maxwell equation in vacuum, and  $\mathbf{E}_S$  is the scattering wave satisfying Eq. (11) generated by the vacuum current. Since the electromagnetic invariants can be nonzero only for the superposition of beams, the vacuum current only exists at the overlap of two beams. In the four-wave coupling, we are interested in the scattering wave with frequency  $\omega_X$  corresponding to the absorption accompanied by the emission (and vice versa) of pump photons for a probe photon, as the other frequency components,  $\omega_X \pm 2\omega_L$ , are usually strongly suppressed [13]. When adding the scattering field to the probe field, vacuum birefringence manifests itself as the induced ellipticity. To detect the signal, an analyzer (polarizer) is set before the beam reaches the detector, and only photons polarized perpendicularly to the initial polarization direction can pass.

Equation (10) can be solved using Green's function methods. For the detector at far field  $\mathbf{r} = (R \cos \theta, R \sin \theta \cos \varphi, R \sin \theta \sin \varphi)$  with the small scattering angle  $\theta$ , the generated field is the superposition of the vacuum current source contribution in the interaction region  $\mathbf{r}_0 = (x', r' \cos \beta, r' \sin \beta)$  at the retarded time  $t_{rect} = t - |\mathbf{r} - \mathbf{r}_0| \approx t - R + x' \cos \theta + r' \sin \theta \cos(\varphi - \beta)$ , written as

$$E_{Sy}(t, \theta, \varphi) = -\frac{3\sqrt{2}\xi k_X^2}{8\pi R} \int_{-\infty}^{\infty} \int_0^{\infty} \int_0^{2\pi} e^{-i\omega_X(t-R)} \times h[x', t - R + x' \cos \theta + r' \sin \theta \cos(\varphi - \beta)] \times e^{-i(\omega_X \cos \theta - k_X)x'} A_L^2(r', t_{rect} - x') A_X(r', x') \times e^{-i\omega_X r' \sin \theta \cos(\varphi - \beta)} dx' r' dr' d\beta. \quad (12)$$

It can be seen that the transverse integration takes a similar form of the Fraunhofer diffraction, where the polarized vacuum can be considered to diffract the probe, and the optical laser  $A_L^2$  plays the role of an aperture. The scattering wave has a different angular distribution for the different choices

of the beams' waists, known as the vacuum diffraction effect [31–34]. For  $w_X > w_L$ , the scattering wave would have a larger angular distribution than the XFEL probe, and at a certain angle, the scattering signal could be stronger than the XFEL background and be discernible. For a given XFEL photon number, a larger  $w_X$  means a larger diffraction angle and a larger discernible photons rate, but the total signal strength decreases because fewer XFEL photons are included in the interaction region. Here we use the XFEL with a much smaller waist than the optical pump to get the maximum total scattering photon number, since the signal's polarization is the detection signature and we do not have to spatially separate it from the XFEL background. In this way, the scattering wave has the same angular distribution as the XFEL background, and we do not account for the transverse structure of the optical pump laser, but instead consider its longitudinal structure  $1/[1 + (t_{\text{rect}} - x')^2/4x_L^2]$ .

Now we consider the longitudinal integration in Eq. (12). For the beams with many periods, we have  $x'\theta^2$ ,  $r'\theta \ll \tau_X$ ,  $\tau_L$  so that the temporal shape

$$\begin{aligned} & h[x', t - R + x' \cos \theta + r' \sin \theta \cos(\varphi - \beta)] \\ & \approx h(x', t - R + x') = h_L^2(t - R + 2x')h_X(t - R), \end{aligned} \quad (13)$$

showing that the scattering signal wave has the same temporal profile  $h_X(t-R)$  as the probe XFEL. When the probe at longitudinal position  $x'$  meets the pump at time  $t-R+x'$ , it generates the radiation at time  $t$ . The scattering signal is the superposition of vacuum current source contribution at different longitudinal positions, and the extent of the interaction volume depends on the pump's temporal profile  $h_L^2(t-R+2x')$ : for a given  $t-R$ ,  $2x'$  can vary in the range of  $\tau_L$ . Additionally, the interaction volume also depends on the pump's longitudinal spatial profile. For a traditional Gaussian envelope with the decaying focal terms  $1/(1+x'^2/x_L^2)$ , the vacuum current source becomes weak for large  $x'$  far away from the focus; thus the effective interaction length is limited by the pump's Rayleigh length. However, as the probe at different longitudinal position  $x'$  meets the pump at the different time, things are different when the pump's intensity varies with time. For flying focus that travels in the same direction of the probe, the retarded time at different position  $x'$  varies synchronously with the movement of focus  $t_{\text{rect}} - x' \approx t - R$ . As shown in Eq. (12), the decaying focal terms  $1/[1 + (t-R)^2/4x_L^2]$  are irrelevant to the longitudinal position, which means the probe can always experience the most intense part of the pump's spatial profile.

### III. EXPERIMENTAL PARAMETERS AT THE STATION OF EXTREME LIGHT

We use the parameters based on the experiment proposal of the Station of Extreme Light (SEL) at the Shanghai High Repetition Rate XFEL and Extreme Light Facility (SHINE) [35,36]. For the XFEL we choose  $k_X = 12914$  eV,  $\tau_X = 30$  fs, and photon number  $N_X = 10^{12}$ . The x-ray instrument includes the compound refractive lens (CRL) made of beryllium for focusing and the polarizer for purifying the polarity. The high-purity polarizer is realized with channel-cut crystal Si-800, which only reflects photons at a certain polarization

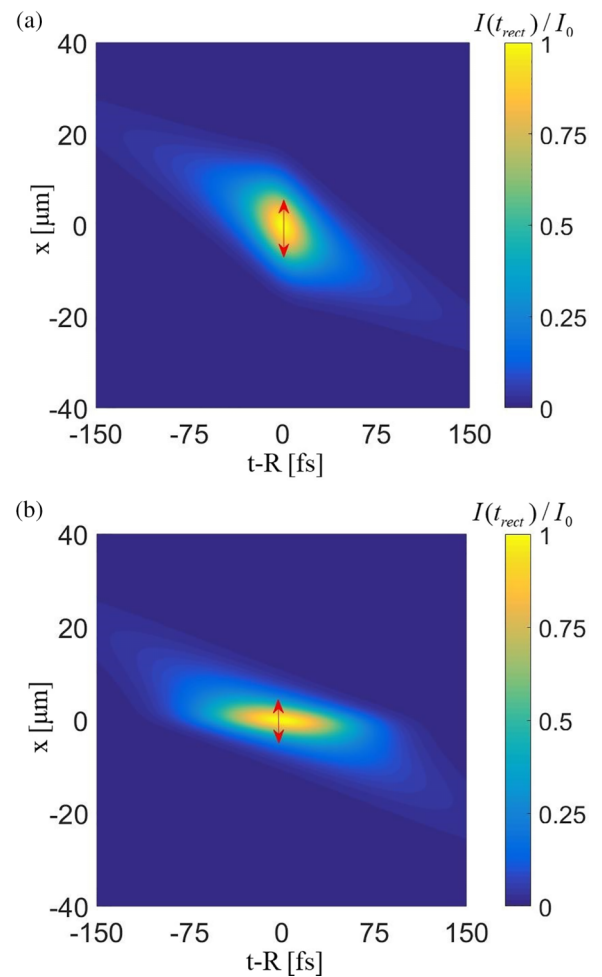


FIG. 1. The pump's on-axis spatial-temporal intensity at the retarded time for (a) flying focus (above) and (b) traditional Gaussian beam (below) with the temporal length  $\tau_L = 75$  fs. The intensity is normalized with  $I_0 = 2.5 \times 10^{23}$  W cm $^{-2}$ . The red line refers to the longitudinal interaction range in Eq. (12).

direction. We chose six-reflection channel cut with an extraction ratio of  $6 \times 10^{-10}$  to ensure the sufficient polarization purity.

For the optical pump laser we choose  $k_L = 1.36$  eV, 4 PW focused to  $w_L = 1$   $\mu\text{m}$ , which has the same peak intensity as the proposed 100 PW, 5  $\mu\text{m}$  at SHINE. We set the temporal length  $\tau_L$  as the variable. As will be shown in the next section, flying focus allows for a long pulse in vacuum birefringence detection. So far flying focus pulses with intensities of the order of  $10^{14}$  W cm $^{-2}$  have been produced [17] and intensities beyond the relativistic threshold  $10^{18}$  W cm $^{-2}$  have been envisaged [21,23]. Since the main technological constraint on the ultrastrong laser is the intensity, in principle a flying focus laser with peak intensity  $2.5 \times 10^{23}$  W cm $^{-2}$  can be obtained.

### IV. RESULTS

Figure 1(a) shows the pump's on-axis intensity at the retarded time  $I(t_{\text{rect}}, x') = I(t-R+x', x')$  as a function of the spatial and temporal coordinate for  $\tau_L = 75$  fs. The red line

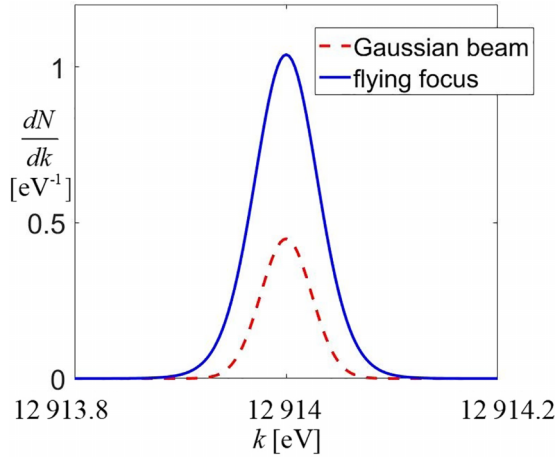


FIG. 2. Spectrum of the scattering photons for the pump with flying focus (filled blue curve) and traditional Gaussian envelope (red dashed line). The temporal length  $\tau_L = 75$  fs.

manifests the integration region over  $x'$  in Eq. (12), and the red line's different location  $t-R$  corresponds to scattering waves at different  $t$ . To compare with the traditional Gaussian beam, Fig. 1(b) gives the result of that with the same parameter. When using the flying focus, the replacement of  $1/(1+x'^2/x_L^2)$  with  $1/[1+(t-R)^2/4x_L^2]$  manifests that the scattering wave's effective temporal length, instead of the interaction length, is limited by the pump's Rayleigh length. It can be seen that for flying focus, the pump has the narrower extent in the  $t-R$  direction, but a wider extent in the  $x$  direction. As mentioned earlier, the generated scattering wave has the same temporal length  $\tau_X = 30$  fs as the probe, which means the intensity distribution at  $|t-R| > 30$  fs has little significance, so that the flying focus with the longer extent in the  $x$  direction has more advantages. With the growth of  $\tau_L$ , for flying focus, the interaction length grows simultaneously, while for a traditional Gaussian beam, the interaction length is limited by the pump's Rayleigh length. Therefore, when  $\tau_L \gg x_L$ , the interaction volume with flying focus of the order  $\tau_L$  can have a much larger spatial extent than the traditional Gaussian beam of the order  $x_L$ .

Now we consider the property of the scattering wave. From the uncertainty relationship, a shorter temporal length limited by  $1/[1+(t-R)^2/4x_L^2]$  means a wider frequency bandwidth for the scattering wave. As vacuum birefringence corresponds to the scattering process of absorption accompanied by the emission of one pump photon, the generated scattering wave's frequency can vary in the range of the pump's bandwidth compared to the XFEL. For the traditional Gaussian beam, its bandwidth is dominated by the Gaussian temporal shape  $h_L(t+x')$ , where a longer temporal length corresponds to a narrower bandwidth. (For a chirped pulse  $h_L(t+x') = \exp[-(t+x')^2(1+iC)/\tau_L^2]$ ,  $h_L^2$  changes to  $h_L h_L^*$  and it still gives the same result with the nonchirp case.) However, for flying focus, the spatial-temporal coupling term  $A_L(r', t-x')$  is independent of  $h_L^2$ , so that it can provide a wide bandwidth even for the long pulse. From the origin of flying focus, it comes from the time-dependent phase at different longitudinal positions [20]. Figure 2 shows the scattering wave's band-

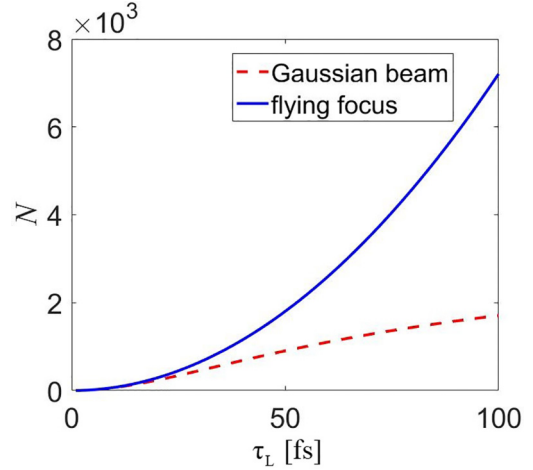


FIG. 3. Dependency of scattering photon number on the pulse duration for flying focus (filled blue curve) and traditional Gaussian envelope (red dashed line) with  $I_L = 2.5 \times 10^{23}$  W cm $^{-2}$ ,  $\tau_X = 30$  fs, and  $x_L = 3.45$   $\mu$ m.

width for  $\tau_L = 75$  fs. For the traditional Gaussian beam, the scattering wave's bandwidth is almost unchanged, still being  $1/\tau_X = 0.02$  eV, while for the flying focus, it can vary in the wider range  $1/x_L = 0.06$  eV.

When using the flying focus, from Eq. (12), for the XFEL with a much smaller waist than the pump, the vacuum birefringence signal can be calculated analytically, normalized with  $N_X$  and  $\tau_L$  as

$$N = \frac{9\pi N_X}{137^2(45\pi)^2 32} \left(\frac{I_L}{I_{cr}}\right)^2 k_X^2 \tau_L^2 g(\tau_X), \quad (14)$$

where

$$g(\tau_X) = \frac{8x_L^2}{\tau_X^2} - \left(\frac{8x_L^2}{\tau_X^2} - \frac{1}{2}\right) \sqrt{\frac{8\pi x_L^2}{\tau_X^2}} \times \exp\left(\frac{8x_L^2}{\tau_X^2}\right) \operatorname{erfc}\left(\sqrt{\frac{8x_L^2}{\tau_X^2}}\right). \quad (15)$$

For the XFEL with small temporal length  $\tau_X < 2x_L$ , we have  $g(\tau_X) \approx 1$ . This equation manifests that to maximize the signal, a strong intensity  $I_L$  is required, so that we use the tightly focused laser, and the XFEL is an ideal probe since it can provide both the large frequency  $k_X$  and the appreciable photon numbers  $N_X$ . Meanwhile, the scattering signal can be greatly increased with the longer temporal length  $\tau_L$ . However, for the traditional Gaussian envelope, the quadratic relationship between  $N$  and  $\tau_L$  is only valid for small  $\tau_L$  when the diffraction of the pump is not important (the detailed expression can be seen in [31]). A smaller waist means a smaller Rayleigh length  $x_L$ , and when  $\tau_L \gg x_L$ ,  $x_L$  becomes the length scale, which means the strong intensity and the long interaction length cannot be provided simultaneously. Our flying focus can overcome this limitation. The dependency of the scattering photon number on the pump's temporal length is shown in Fig. 3. It can be seen that flying focus can greatly enhance the signal when the pump's temporal length is larger than its Rayleigh length. Therefore, as shown in Fig. 4(a), the



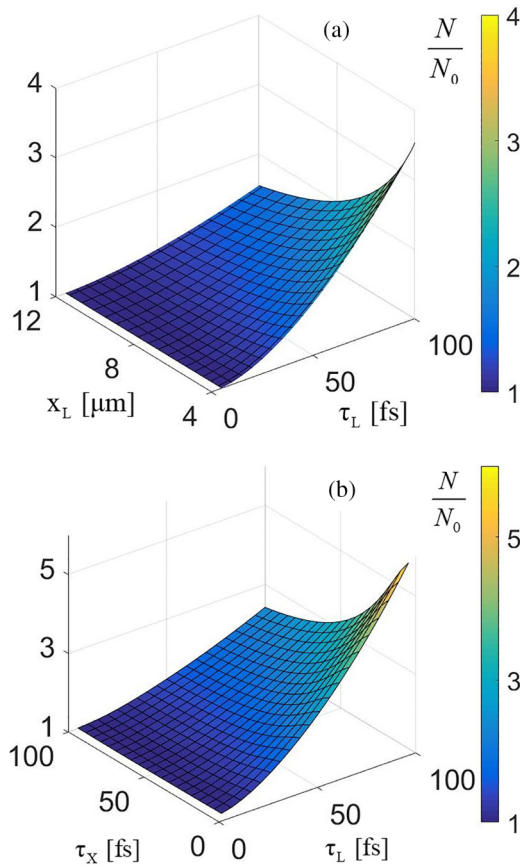


FIG. 4. Dependency of the ratio of the signal by the flying focus  $N$  to the signal by the stationary focus  $N_0$  on (a) the pump's duration  $\tau_L$  and the pump's Rayleigh length  $x_L$  with  $I_L = 2.5 \times 10^{23} \text{ W cm}^{-2}$ , and  $\tau_x = 30 \text{ fs}$ , and (b) the pump's duration  $\tau_L$  and the probe's duration  $\tau_x$  with  $I_L = 2.5 \times 10^{23} \text{ W cm}^{-2}$  and  $x_L = 3.45 \mu\text{m}$ .

ratio of the signal by the flying focus  $N$  to the signal by the stationary focus  $N_0$  becomes larger for a smaller Rayleigh length. Besides, From Fig. 1(a) we can see that most of the flying focus pump energy distributes in the range about  $|t-R| < \tau_x$ ,

and the energy in the range about  $|t-R| < x_L$  contributes to the signal. Therefore, as shown in Fig. 4(b), the flying focus is more superior to the stationary focus for a smaller XFEL temporal length.

In many papers, such as [37], it is proposed to detect vacuum birefringence in the regime  $\tau_L < x_L$  to make full use of the pump laser's energy, where infinite Rayleigh-length approximation of ignoring the pump's diffraction is widely used. Here flying focus extends the experimental parameters of using the long pulse  $\tau_L \gg x_L$ , and infinite Rayleigh length is automatically satisfied. For the pump pulse, Eq. (14) shows that the birefringence signal is only relevant to its energy  $I_L \tau_L$ ; therefore for a given pulse energy, flying focus provides a unique approach to detect vacuum birefringence with weaker intensity and longer temporal length. In high-power laser systems, the ultrashort beam is usually derived from the compression. For example, the ELI (Extreme Light Infrastructure) L1 beamline compresses the beam from 2–3 ps to less than 15 fs [38]. With the flying focus, the compression of the beam may not be necessary, which can make the detection of vacuum birefringence easier.

## V. CONCLUSIONS

We investigate vacuum birefringence in the head-on collision between a XFEL probe and an optical laser pump. We propose a method of detecting the signal using the flying focus laser with the focus speed  $-c$ . The signal can be greatly enhanced when the pump's temporal length is larger than its Rayleigh length. It partly overcomes the drawback of short interaction length for an ultrastrong laser in the detection of vacuum birefringence, which may lead to the experimental observation of this effect.

## ACKNOWLEDGMENTS

This work was supported by the Ministry of Science and Technology of the People's Republic of China (Grant No. 2018YFA0404803) and the National Natural Science Foundation of China (Grant No. 11935008).

- 
- [1] W. Heisenberg and H. Euler, *Z. Phys.* **98**, 714 (1936).  
 [2] J. Schwinger, *Phys. Rev.* **82**, 664 (1951).  
 [3] J. J. Klein and B. Nigam, *Phys. Rev.* **135**, B1279 (1964).  
 [4] Z. Bialynicka-Birula and I. Bialynicki-Birula, *Phys. Rev. D* **2**, 2341 (1970).  
 [5] S. L. Adler, *Ann. Phys.* **67**, 599 (1971).  
 [6] R. Battesti, J. Beard, S. Boser, N. Bruyant, D. Budker, S. A. Crooker, E. J. Daw, V. V. Flambaum, T. Inada, I. G. Irastorza *et al.*, *Phys. Rep.* **765**, 1 (2018).  
 [7] C. N. Danson, C. Haefner, J. Bromage, T. Butcher, J.-C. F. Chanteloup, E. A. Chowdhury, A. Galvanauskas, L. A. Gizzi, J. Hein, D. I. Hillier *et al.*, *High Power Laser Sci. Eng.* **7**, e54 (2019).  
 [8] K. A. Tanaka, K. M. Spohr, D. L. Balabanski, S. Balascuta, L. Capponi, M. O. Cernaianu, M. Cuciuc, A. Cucoanes, I. Dancus, A. Dhal *et al.*, *Matter Radiat. Extremes* **5**, 024402 (2020).  
 [9] E. Iacopini and E. Zavattini, *Phys. Lett. B* **85**, 151 (1979).  
 [10] S. Askenazy, C. Rizzo, and O. Portugall, *Phys. B (Amsterdam)* **294**, 5 (2001).  
 [11] J.-S. Wu, W.-T. Ni, and S.-J. Chen, *Class. Quantum Grav.* **21**, S1259 (2004).  
 [12] D. Tommasini and H. Michinel, *Phys. Rev. A* **82**, 011803 (2010).  
 [13] B. King and C. H. Keitel, *New J. Phys.* **14**, 103002 (2012).  
 [14] S. Ataman, *Phys. Rev. A* **97**, 063811 (2018).  
 [15] H.-P. Schlenvoigt, T. Heinzl, U. Schramm, T. E. Cowan, and R. Sauerbrey, *Phys. Scr.* **91**, 023010 (2016).  
 [16] A. Sainte-Marie, O. Gobert, and F. Quere, *Optica* **4**, 1298 (2017).  
 [17] D. H. Froula, D. Turnbull, A. S. Davies, T. J. Kessler, D. Haberberger, J. P. Palastro, S.-W. Bahk, I. A. Begishev, R. Boni, S. Bucht, J. Katz, and J. L. Shaw, *Nat. Photonics* **12**, 262 (2018).

- [18] T. T. Simpson, D. Ramsey, P. Franke, K. Weichman, M. V. Ambat, D. Turnbull, D. H. Froula, and J. P. Palastro, *Opt. Express* **30**, 9878 (2022).
- [19] J. P. Palastro, J. L. Shaw, P. Franke, D. Ramsey, T. T. Simpson, and D. H. Froula, *Phys. Rev. Lett.* **124**, 134802 (2020).
- [20] D. Ramsey, A. Di Piazza, M. Formanek, P. Franke, D. H. Froula, B. Malaca, W. B. Mori, J. R. Pierce, T. T. Simpson, J. Vieira, M. Vranic, K. Weichman, and J. P. Palastro, *Phys. Rev. A* **107**, 013513 (2023).
- [21] M. Formanek, D. Ramsey, J. Palastro, and A. Di Piazza, *Phys. Rev. A* **105**, L020203 (2022).
- [22] D. Ramsey, P. Franke, T. T. Simpson, D. H. Froula, and J. P. Palastro, *Phys. Rev. E* **102**, 043207 (2020).
- [23] A. Di Piazza, *Phys. Rev. A* **103**, 012215 (2021).
- [24] J. R. Pierce, J. P. Palastro, F. Li, B. Malaca, D. Ramsey, J. Vieira, K. Weichman, and W. B. Mori, *Phys. Rev. Res.* **5**, 013085 (2023).
- [25] E. Heyman and T. Melamed, *IEEE Trans. Antennas Propag.* **42**, 518 (1994).
- [26] A. April, in *Coherence and Ultrashort Pulse Laser Emission*, edited by F. J. Duarte (IntechOpen, London, 2010), Chap. 16.
- [27] T. Heinzl, B. Liesfeld, K.-U. Amthor, H. Schwöerer, R. Sauerbrey, and A. Wipf, *Opt. Commun.* **267**, 318 (2006).
- [28] V. Dinu, T. Heinzl, A. Ilderton, M. Marklund, and G. Torgrimsson, *Phys. Rev. D* **89**, 125003 (2014).
- [29] F. Karbstein and R. R. O. Weernink, *Phys. Rev. D* **104**, 076015 (2021).
- [30] A. Fedotov, A. Ilderton, F. Karbstein, B. King, D. Seipt, H. Taya, and G. Torgrimsson, *Phys. Rep.* **1010**, 1 (2023).
- [31] F. Karbstein, H. Gies, M. Reuter, and M. Zepf, *Phys. Rev. D* **92**, 071301 (2015).
- [32] F. Karbstein and E. A. Mosman, *Phys. Rev. D* **100**, 033002 (2019).
- [33] B. Jin, B. Shen, and D. Xu, *Phys. Rev. A* **106**, 013502 (2022).
- [34] B. King, A. Di Piazza, and C. H. Keitel, *Nat. Photonics* **4**, 92 (2010).
- [35] B. Shen, Z. Bu, J. Xu, T. Xu, L. Ji, R. Li, and Z. Xu, *Plasma Phys. Controlled Fusion* **60**, 044002 (2018).
- [36] D. Xu, B. Shen, J. Xu, and Z. Liang, *Nucl. Instrum. Methods. Phys. Res., Sect. A* **982**, 164553 (2020).
- [37] E. A. Mosman and F. Karbstein, *Phys. Rev. D* **104**, 013006 (2021).
- [38] P. Bakule, R. Antipenkov, J. Novák, F. Batysta, R. Boge, J. Tyler Green, Z. Hubka, M. Greco, L. Indra, A. Špaček *et al.*, in *High Intensity Lasers and High Field Phenomena* (Optica Publishing Group, Washington, DC, 2020), p. HF1B. 7.